Ethylene decomposition on Ir(111): Initial path to graphene formation†

Holly Tetlow*, Joel Posthuma de Boer‡, Ian J. Ford[a], Dimitri D. Vvedensky‡, Davide Curcio[b], Luca Omiciuolo[b], Silvano Lizzit[c], Alessandro Baraldi[bcd], and Lev Kantorovich*

Abstract

The complete mechanism behind the thermal decomposition of ethylene (C_2H_4) on Ir(111), which is the first step of graphene growth, is established for the first time employing a combination of experimental and theoretical methods. High-resolution x-ray photoelectron spectroscopy was employed, along with calculations of core level binding-energies, to identify the surface species and their evolution as the surface temperature is increased. To understand the experimental results, we have developed a reaction sequence between the various C_nH_m species, from ethylene to C monomers and dimers, based on *ab initio* density functional calculations of all the energy barriers and the Arrhenius prefactors for the most important processes. The resulting temperature evolution of all species obtained from the simulated kinetics of ethylene decomposition agrees with photoemission measurements. The molecular dissociation mechanism begins with the dehydrogenation of ethylene to vinylidene (CH_2C), which is then converted to acetylene (CHCH) by the removal and addition of an H atom. The C-C bond is then broken to form methylidyne (CH), and in the same temperature range a small amount of ethylidyne (CH_3C) is produced. Finally methylidyne dehydrogenates to produce C monomers that are available for the early stage nucleation of the graphene islands.

*Physics Department, King's College London, London, WC2R 2LS, United Kingdom.

‡The Blackett Laboratory, Imperial College London, London SW7 2AZ, United Kingdom.

[a]Department of Physics and Astronomy and London Centre for Nanotechnology, University College London, Gower Street, London WC1E 6BT, United Kingdom.

[b]Physics Department, University of Trieste, Via Valerio 2, 34127 Trieste, Italy.

[c]Elettra – Sincrotrone Trieste S.C.p.A., AREA Science Park, S.S. 14 km 163.5, 34149 Trieste, Italy

[d]IOM-CNR, Laboratorio TASC, AREA Science Park, S.S. 14 km 163.5, 34149 Trieste, Italy.

† *Electronic Supplementary Information (ESI) available: [Alternative species geometries and alternative NEB reaction mechanisms, as well as the NEB energy profiles for all reactions, their pre factors and vibrational frequency calculations. Also a detailed description of the kMC code.]. See DOI: 10.1039/b000000x/*

1 Introduction

Graphene offers an impressive array of properties, but in order for these to be harnessed for applications, it is vital to understand and exploit methods for the large-scale production of high quality material. The most promising for technological applications are epitaxial methods [1], including chemical vapour deposition (CVD), which can be performed either at a constant temperature [2, 3, 4, 5, 6] or at varying temperature (temperature-programmed growth (TPG)). [7, 8, 2, 5, 9, 10] In these methods, hydrocarbons are deposited onto a transition-metal surface at high temperatures to induce the decomposition of the hydrocarbons, leading to the formation of various C_nH_m species that become involved in the nucleation and growth of monolayer graphene islands.

However, the mechanisms of this rather complicated chain of chemical reactions are not fully understood at the atomic level. Little is known about the atomistic processes involved in the conversion of the initial hydrocarbon feedstock into carbon for graphene growth.

Some experimental and theoretical work has attempted to determine the reaction steps for the adsorption of ethylene on a transition-metal surface and its subsequent decomposition to release C atoms. These methods include, in particular, TPG, where the deposition, typically performed at room temperature, is followed by subsequent heating to promote growth.

In a previous experiment [11] different hydrocarbon species were identified using fast-XPS [12] (x-ray photoelectron spectroscopy) on the Ir(111) surface during the thermal evolution of adsorbed ethylene (CH_2CH_2). The results suggested that ethylene is first converted to ethylidene ($CHCH_3$), prior to a series of dehydrogenation reactions that lead to the presence of carbon on the surface in the form of monomers as well as clusters with a peculiar dome shape [13], eventually leading to graphene at temperatures higher than 950 K.

There have also been several theoretical attempts to understand the early stages of hydrocarbon decomposition on catalytic surfaces. On Cu(001) and Cu(111) [14, 15], the energetics of the direct dehydrogenation of adsorbed methane and ethylene were modelled using density functional theory (DFT). Only dehydrogenation reactions were considered, i.e. the hydrogen atoms were removed sequentially to become adsorbed onto the surface, leaving behind a carbon cluster. However, the large energy barriers found for these reactions suggested that the mechanism based exclusively on direct dehydrogenation may be energetically unfavourable.

Alternative pathways to dehydrogenating hydrocarbons have also been considered. [16, 17, 18, 19] The removal of a single H atom from ethylene adsorbed on the Pt(111) and Pd(111) surfaces was investigated by considering various reaction processes. [17] An H atom could be added or removed from either of the two C atoms in the ethylene molecule, or it could move from one carbon atom to the other (hydrogenation, dehydrogenation and isomerisation reactions, respectively). Building on this, the energy barriers for these reactions were employed in a kinetic Monte Carlo scheme to find the most favourable mechanism for the removal of the first H atom from ethylene. [16] Ethylene was found to undergo two dehydrogenation reactions to form vinylidene (CH_2C), before being hydrogenated to ethylidyne (CH_3C). However, this work did not include the possibility of breaking the C-C bond in ethylene and intermediate species, which must be a pathway to producing C monomers. These reactions have been included in similar

work on the decomposition of C_nH_m species on the Pt(111) and Pt(210) surfaces. [19, 20] In this rather extensive study all reactions (including hydrogenation, dehydrogenation, isomerisation and C-C cleavage) were included in a scheme involving reactions between all hydrocarbons C_nH_m from CH_3CH_3 to C monomers. The energy barriers for each reaction were calculated and used to make qualitative conclusions about the reaction sequence. From this it was suggested that C-C cleavage of certain species would be possible. However, the kinetics of the reaction was not studied, and the results were obtained by judging the likelihood of various reactions in the sequence based only on the energy barriers, with no experimental input.

Therefore, the detailed mechanism of ethylene decomposition as the first stage of graphene growth remains largely unknown. The main objective of the work reported here is to fill in this gap by determining the complete ethylene decomposition pathway on Ir(111) by using a combination of experimental methods and a comprehensive tailored theoretical framework for the energy landscape and reaction kinetics. The outline of this paper is as follows. We discuss XPS C 1s core level spectroscopy experiments, performed while increasing the temperature and designed to understand the role of the initial ethylene coverage and to obtain spectroscopic signatures of the main distinct species on the surface as the decomposition proceeds. We then discuss the results of DFT calculations for various C_nH_m species that may appear on Ir(111) during ethylene decomposition. To guide the interpretation of C 1s core level spectra measured after annealing the system at selected temperatures, we compared the experimental and calculated C 1s core level shifts for the different C_nH_m species. This enabled us to determine the evolution of these species during heating. To understand the ethylene decomposition pathway(s), the complete reaction scheme connecting ethylene with carbon monomers and dimers was developed. This includes dehydrogenation, hydrogenation, isomerisation and carbon cleavage reactions, for all of which the transition barriers were calculated using *ab initio* DFT. For the reactions which are judged by the comparison of the DFT and experimental binding energies to be the most important to the decomposition pathway, Arrhenius prefactors were calculated with DFT using classical transition-state theory. [21, 22] These results have allowed us to determine the rate constants for all of the allowed reactions and in turn create a kinetic Monte Carlo simulation to reveal the detailed kinetics of ethylene decomposition, and to propose the most likely pathway for the conversion of ethylene to carbon prior to graphene growth. The relative concentrations of the various hydrocarbon species found in this way are in good agreement with the corresponding quantitative determination from the C 1s core level data.

2 Experimental Methods

The Ir(111) sample used in this experiment was a 8 mm diameter single crystal disk. Sample cleaning, preparation and characterisation were carried out at the SuperESCA undulator beamline of the Elettra synchrotron radiation facility (Basovizza - Italy). Due to the high photon flux, the SuperESCA beamline is specifically designed for fast-XPS spectra experiments. Together with a 150 mm mean radius hemispherical electron energy analyser from SPECS, equipped with an in-house developed delay-line detector, the setup allows for fast (100 ms per spectra) and

high-resolution XPS (ΔE=40 meV at photon energy $h\nu$ =400 eV). A manipulator equipped with a cold finger and W heating filaments positioned close to the back of the sample allows for temperature resolved experiments to be carried out under Ultra High Vacuum (UHV) conditions, with base pressures between 1×10^{-10} and 2×10^{-10} mbar. The sample was cleaned by means of repeated cycles of Ar^+ ion sputtering and annealing to 1400 K, followed by oxygen and hydrogen treatment to remove the carbon contaminants and the residual chemisorbed oxygen, respectively. The whole procedure was repeated until the C1s and O1s regions of the core-level spectra did not show any trace of contaminants. In these conditions the Ir4f7/2 spectrum spectrum showed a surface core level shift of -550 meV. [23] C 1s core level spectra were acquired in normal emission geometry, using a photon energy of 400 eV. The low energy electron diffraction (LEED) experiments were performed in the UHV chamber (base pressure 1×10^{-10} mbar) of the Surface Science Laboratory at Elettra-Sincrotrone Trieste, also equipped with a manipulator that allows for temperature control by using a cold finger for cooling and W filaments for radiative heating or electron bombardment. LEED experiments were performed using a Fisons rear-view electron optical system.

3 Theoretical Methods

The geometry optimisation and nudged elastic band (NEB) calculations [24, 25, 26, 27] have been performed using density functional theory with the CP2K code [28]. Goedecker-Teter-Hutter (GTH) [29] pseudopotentials were used as well as the generalised gradient approximation (GGA) with the PBE exchange-correlation functional. [30] Van der Waals forces are included with the DFT-D3 method. [31] The optimised m-DZVP basis set [32] was used for all atoms together with a plane wave cutoff energy of 300 Ry. Geometries were relaxed until forces on atoms were less than 0.038 eV/Å.

For the geometry relaxations on the Ir(111) surface, a slab consisting of 4 layers of an 8×8 periodic lattice has been used, with a vacuum gap of 15 Å. The bottom two layers remain frozen to the bulk geometry and the others are allowed to relax. For the NEB calculations between 2 and 7 layers were used in order to achieve convergence of the energy barriers for the most crucial reactions. In this case the 1 or 2 bottom layers were frozen. More details are provided in the supporting information (SI).

For the adsorbed hydrocarbon species C_nH_m, the adsorption energy E_{bind} is calculated using the formula:

$$E_{bind} = E_{\mathrm{C}_n\mathrm{H}_m+\mathrm{Ir}} - E_{\mathrm{Ir}} - E_{\mathrm{C}_n\mathrm{H}_m}, \tag{1}$$

where $E_{\mathrm{C}_n\mathrm{H}_m+\mathrm{Ir}}$ is the energy of the hydrocarbon adsorbed onto the surface, $E_{\mathrm{C}_n\mathrm{H}_m}$ is the energy of the hydrocarbon molecule in the vacuum, and E_{Ir} is the energy of the bare Ir(111) surface. For these adsorption energy calculations the basis set superposition error (BSSE) correction has been employed based on the counterpose method. [33]

Depending on the system complexity, between 7 to 13 images have been used in our NEB calculations of species diffusion and for elementary reactions to find the minimum energy pathway

between the initial and final states in each case. The climbing image NEB method is employed to ensure the saddle point corresponding to the correct energy barrier is properly located. [27]

The kinetic Monte Carlo (kMC) simulation is initialised by randomly placing ethylene molecules on a surface grid consisting of 7500 sites. At each kMC step all possible reactions for each species are determined based on their local environment and a list of all possible moves (processes) is compiled. The rates for each reaction are given in the Arrhenius form, $R = \nu \exp(-E/k_B T)$, where E is the calculated energy barrier, k_B the Boltzmann constant, T the temperature and ν the attempt frequency. Based on the algorithm of Bortz, Kalos, and Lebowitz, (BKL algorithm) a reaction from the list is selected [34]. The simulation time is to be updated by calculating a variable time step Δt_{var}. Since the temperature is continuously ramped throughout the simulation, the rates of individual processes become time-dependent. Hence, the time step is determined using a time-dependent algorithm [35] based on the time-dependent residence rate. Since the diffusion of most of the species does not play the dominant role in the reaction kinetics, the species can be rearranged randomly at each step in order to replicate their diffusion. This speeds up the simulation time considerably. The details of the kMC code including species diffusion, are provided in the SI.

In order to determine the pre-exponential factors in the rate expressions for some of the reactions, we calculated the vibrational frequencies associated with all atoms (that are allowed to relax) in our cell for the initial, transition and final state geometries. For the transition state, which is a saddle point, there will be one imaginary frequency associated with the configuration and hence, in contrast to the number of frequencies $3N$ for the initial and final states, there will be $3N-1$ frequencies associated with the transition state. Then the prefactor ν_{ij} in the corresponding Arrhenius expression for the transition $i \to j$ between two states of a system (i.e. the attempt frequency) is obtained using [21, 22]

$$\nu_{ij} = \frac{\prod_{k=1}^{3N} f_k^{(i)}}{\prod_{k=1}^{3N-1} f_k^{(\mathrm{sad})}}, \tag{2}$$

where $\{f_k^{(i)}\}$ and $\{f_k^{(\mathrm{sad})}\}$ are the vibrational frequencies in the initial (i) and saddle point (sad) states, respectively. The calculation of the prefactor ν_{ji} for the reverse reaction requires calculating vibrational frequencies $\left\{f_k^{(j)}\right\}$ in the state j which replace the frequencies in the numerator in Eq. (2).

The core level shift associated with a particular C atom of a C_nH_m species is calculated [36] as the difference between the energy of the system with a hole in the C atom core level, $E(n_c - 1)$, with the core electron added to the valence band, and the energy of the neutral unexcited system, $E(n_c)$:

$$E_{CLS} = E(n_c - 1) - E(n_c)\ . \tag{3}$$

By appropriately displacing atoms in the C 1s core-hole excited state and using the calculated atomic forces to work out the corresponding dynamical matrix, vibrational frequencies corresponding to XPS peaks satellites were calculated.

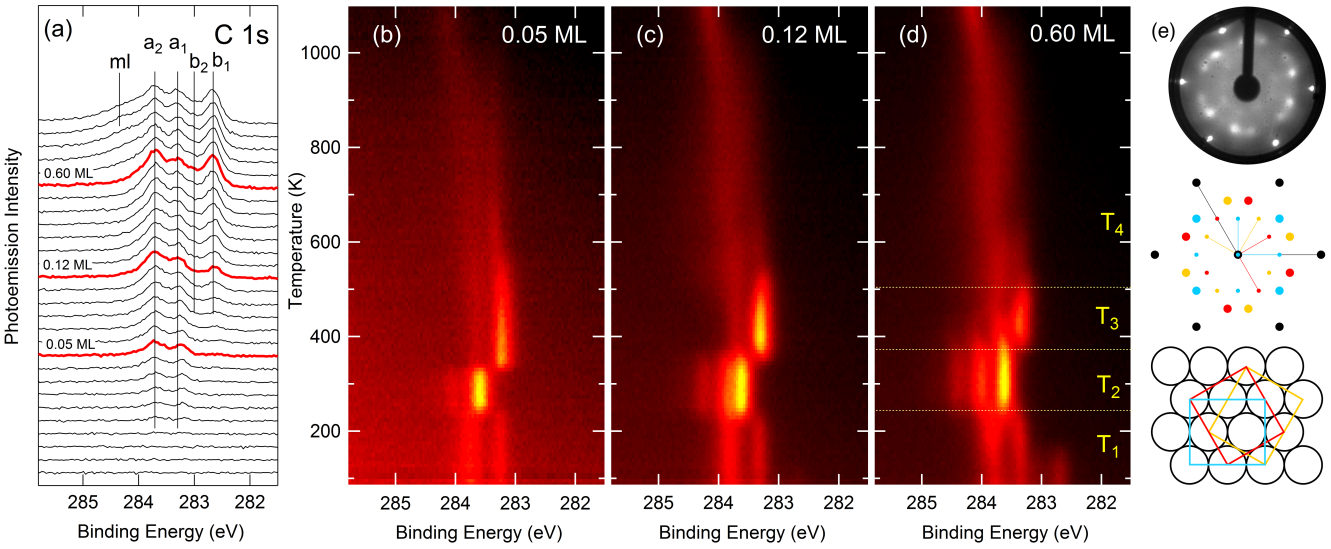

Figure 1: (a) XPS C 1s spectra acquired during ethylene uptake at 90 K. The three spectra highlighted in red correspond to the three coverages used throughout the experiment. (b-d) 2D plots corresponding to the TP-XPS C 1s spectral series acquired during the annealing from 90 K to high temperature for the three different ethylene coverages. Each horizontal cut in the figures corresponds to a single photoemission spectrum acquired at a given temperature and its intensity is plotted using a colour scale. (e) (top) LEED pattern acquired at 55 eV after ethylene deposition (0.60 ML) and annealing to 340 K, (middle) simulated diffraction pattern for a c(4×2) superstructure and (bottom) real-space models of possible adsorption geometries associated with the spots of different colours in the middle panel.

4 Results and Discussion

4.1 Photoemission experiments

In all our experiments, the Ir(111) surface was exposed to ethylene (partial pressure between 1×10^{-9} and 2×10^{-9} mbar) at 90 K. The sample was then heated with a temperature ramp of 1.5 Ks^{-1}. In the first part of our investigations, we measured coverage and temperature dependent C 1s XPS spectra to follow the evolution of the system as a function of coverage/temperature, thus providing a first qualitative insight into the chemical environment at each step of the adsorption and dissociation processes and the role of the ethylene surface coverage. In the second stage (reported in the interpretation of core level shifts section) we measured high-resolution C 1s core level spectra after annealing the system to specific temperatures, selected on the basis of the temperature-programmed XPS (TP-XPS) [37] results.

The C coverages for the three stages were estimated by comparing the C 1s core level intensity to the same spectrum acquired for monolayer graphene on Ir(111), [13] so that 1 monolayer (ML) is equivalent to a C atom surface density of $1.567\times10^{15}cm^{-2}$. Figure 1(a) shows a series of C 1s core level spectra acquired during ethylene exposure at 90 K. At the beginning of the uptake we observe two components at 283.3 eV (a_1) and 283.8 eV (a_2) binding energies (BE). Their intensity increases coherently with increasing exposure, preserving a constant intensity ratio and

BE difference. This behaviour can be interpreted in terms of the presence of a single adsorbed molecular species with two non-equivalent C atoms, suggesting that the C-C bond is preserved. By observing the time-resolved XPS spectral series during ethylene adsorption, we were able to detect, above 0.06 ML, the appearance of a new doublet at lower BE due to a different C_2H_m species. While the peak at 282.7 eV BE (b_1) can be easily distinguished, the second peak (b_2) is partially hidden by the $a_{1,2}$ components, and results in a spectral shoulder slightly above 283 eV. With a further increase in the C_2H_4 exposure, a new broad feature can be observed at BEs higher than 284 eV (ml). The observation that in the absence of ethylene flux its intensity rapidly decreases is consistent with the presence of ethylene multilayers. This behaviour is expected for weakly interacting species at the condition of surface adsorption-desorption equilibrium. [38]

In light of the uptake kinetics, we carried out TP-XPS experiments for three different initial ethylene exposures (highlighted in red in Figure 1(a)), corresponding to the presence of just the first $a_{1,2}$ spectral doublet (0.05 ML), a mix of the two doublets (0.12 ML) and the saturated surface, before the multilayer growth (0.60 ML).

In Figure 1(b-d) we report the 2D plots corresponding to the TP-XPS C1s spectral series acquired during annealing from low to high temperature. The chemical evolution occurring at the surface is reflected in strong BE shifts and modifications of the C 1s core level line shape. In particular, we observe sharp transitions at about 250, 380 and 500 K (high coverage series), while at high temperature ($T > 800$ K) the C 1s spectrum smoothly becomes narrower and moves to a higher BE. At the highest temperature, above 900 K, the appearance of a spectral component at a BE of 284.1 eV is observed, which is the fingerprint of the initial nucleation of graphene islands. [11, 13] Most importantly, the C 1s core level evolution is only slightly influenced by the initial C coverage. In fact, the qualitative behaviour is similar for the three selected coverages; only the temperature range of each transition is slightly modified, especially at the lower coverage. The most important spectral change in the low temperature range T_1 (Figure 1(d)) is the decrease of the $b_{1,2}$ components, which transform into $a_{1,2}$. This suggests that, at $T = 90$ K, the lower BE doublet can originate from ethylene species that adsorb without dissociation on the empty sites of the surface initially covered with dissociated C_nH_m species, in agreement with previous assignments [11], and that complete dissociation of CH_2CH_2 takes place only above 200 K.

The TP-XPS spectra are more complicated to interpret in the temperature ranges T_2 and T_3 (Figure 1(d)) because of the overlap of spectral features originating from non-equivalent C atoms of different C_nH_m species with other components due to vibrational splitting. Indeed, it is known that, when measured with high-resolution, the C 1s core level spectra of small hydrocarbon molecules can display vibrational fine structure due to the excitation of C-H vibrational motion in the final state. [39, 40]

For this reason, we performed low-temperature, high-statistics and high-resolution C 1s photoemission experiments after annealing the high-coverage ethylene structure at increasing selected temperatures. The results, when combined with accurate DFT calculated C 1s core level shifts for different chemical species, enabled us to make an accurate interpretation of the different spectral components (reported in the interpretation of CLS core level spectra section) and their evolution with temperature. Also, by comparing the high resolution spectra acquired

before and after annealing, no sensible decrease in C 1s total area was detected. This signifies, in agreement with existing temperature programmed desorption (TPD) measurements [41], that no C containing fragments desorb from the surface, and that the major peak detected by the mass spectrometer corresponds to H_2. In fact the C-containing fragments are expected to be tenaciously held by the Ir(111) surface [41]. This is also in agreement with the adsorption energies calculated in the present study, which suggest that the intermediate species we observe should not desorb (see below). This behaviour is clearly different from what is observed in a similar experiment on Pt(111), where many of the dissociated hydrocarbon fragments have been detected also in TPD experiments. [42]

To assess the geometrical structure of our system, we also performed low-energy electron diffraction (LEED) measurements. Figure 1(e) shows a LEED pattern acquired after ethylene deposition at 90 K up to saturation, followed by annealing at 340 K. Besides the diffraction spots originating from the Ir(111) substrate (black), we observe an additional set of spots related to the superstructure formed by the adsorbed molecules (red, cyan and yellow). The diffraction pattern is interpreted in terms of a c(4×2) structure, with three differently oriented domains, as shown in Figure 1(e). Following this finding, selected theoretical calculations were performed using a c(4×2) unit cell. These are discussed in the supporting information (SI).

4.2 Hydrocarbon species and reaction scheme

To understand the evolution of the different chemical species revealed in the photoemission experiments, we must identify all possible on-surface reactions that might be responsible for the conversion of ethylene molecules into carbon monomers and (possibly) dimers. In these reactions various intermediate C_nH_m species might appear. A reaction scheme for the decomposition of ethylene to carbon, incorporating all processes that the various hydrocarbon species might undergo is shown in Figure 2. We include reactions involving hydrogenation (attachment of a surface-adsorbed H to the species), dehydrogenation (detachment of H from species to the surface) and isomerisation (H atom within the species detaches and reattaches from one C atom to another). In the diagram the breaking of the C-C bond (CB reactions) is also considered for each of the hydrocarbon species with two C atoms. Owing to the inclusion of hydrogen in many of these reactions, the availability of hydrogen atoms on the surface must be taken into account. Adsorbed hydrogen can reattach to any of the molecular species and can also be lost through the formation of molecular hydrogen followed by its desorption from the surface. By calculating reaction rates for all reactions in the scheme, the kinetics can be determined and the preferential route(s) of the ethylene conversion can be deduced.

Before the rates of the various reactions in Figure 2 can be determined, the optimised geometries of all the hydrocarbon species adsorbed on the Ir(111) surface need to be found. These provide the initial and final states in the reactions and are presumed to be responsible for the features in the XPS spectra. Each hydrocarbon species was placed onto the Ir(111) surface and its geometry relaxed using DFT. As multiple geometries were obtained in most cases, the lowest energy configuration was selected as representative for this species and used for further calculation of the respective reaction rates. The geometries for the lowest energy

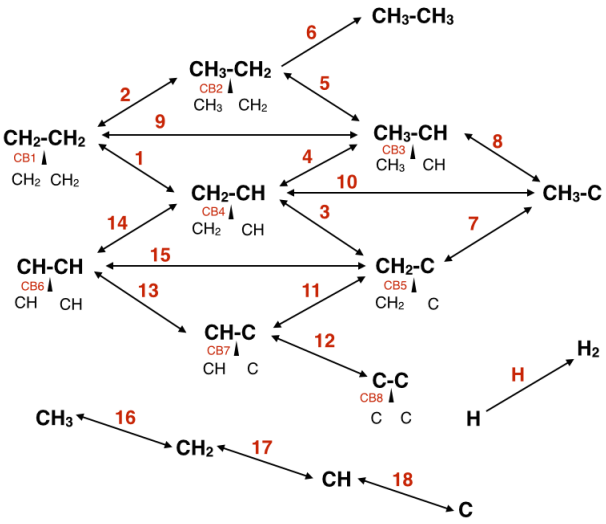

Figure 2: Possible processes considered for the conversion of ethylene CH_2CH_2 into carbon. The upward/downward diagonal arrows represent hydrogenation/dehydrogenation reactions, and the horizontal arrows show isomerisation processes. The reactions are numbered for later reference as in Table 1. Hydrocarbon species containing two carbon atoms may also undergo C-C breaking reactions (CB) to form C monomer species, as indicated beneath each species symbol with small vertical arrows. This diagram is similar to the scheme proposed previously in Ref. [19].

configuration of each C_nH_m species are shown in Figure 3 along with their binding energies. Other configurations we found are shown in the SI.

For ethylene (CH_2CH_2) we find that the lowest energy configuration is obtained when the molecule is in the bridge position, between two Ir atoms. This allows each C atom to be bonded to four atoms. The species CH_2CH, CH_3CH, CH_3C and CH_2C are centred on either the fcc or hcp three-fold hollow sites. The difference in adsorption energy between attachment at fcc and hcp sites is negligible. For CH_3CH_2 the CH_2 group is attached to the top site, while the CH_3 is suspended away from the surface. CH_3CH_3 is only weakly interacting with the surface. The structure of CHCH has each of the CH groups in a bridge site. Compared to CHCH, in CHC the C atom without hydrogen shifts towards the other to rest in the hollow site. The remaining hydrogen atom orientates itself further away from the surface. For the carbon dimer, CC, the C atoms are found in both the hcp and fcc sites, and are connected across the bridge site. For the single C species we find that the lowest energy geometries for CH_3 and CH_2 are when they are positioned on the top and bridge sites, respectively. This allows the C atoms to form four bonds each. CH and C both relax onto the hcp site. For C this is 0.2 eV lower in energy than for the fcc site geometry.

4.3 Energy barriers

To find the preferential reaction paths in the process of ethylene decomposition, the corresponding energy barriers for all forward and backward reactions shown in Figure 2 need to be calculated. This requires understanding the energetics of adsorbed hydrogen atoms, since when

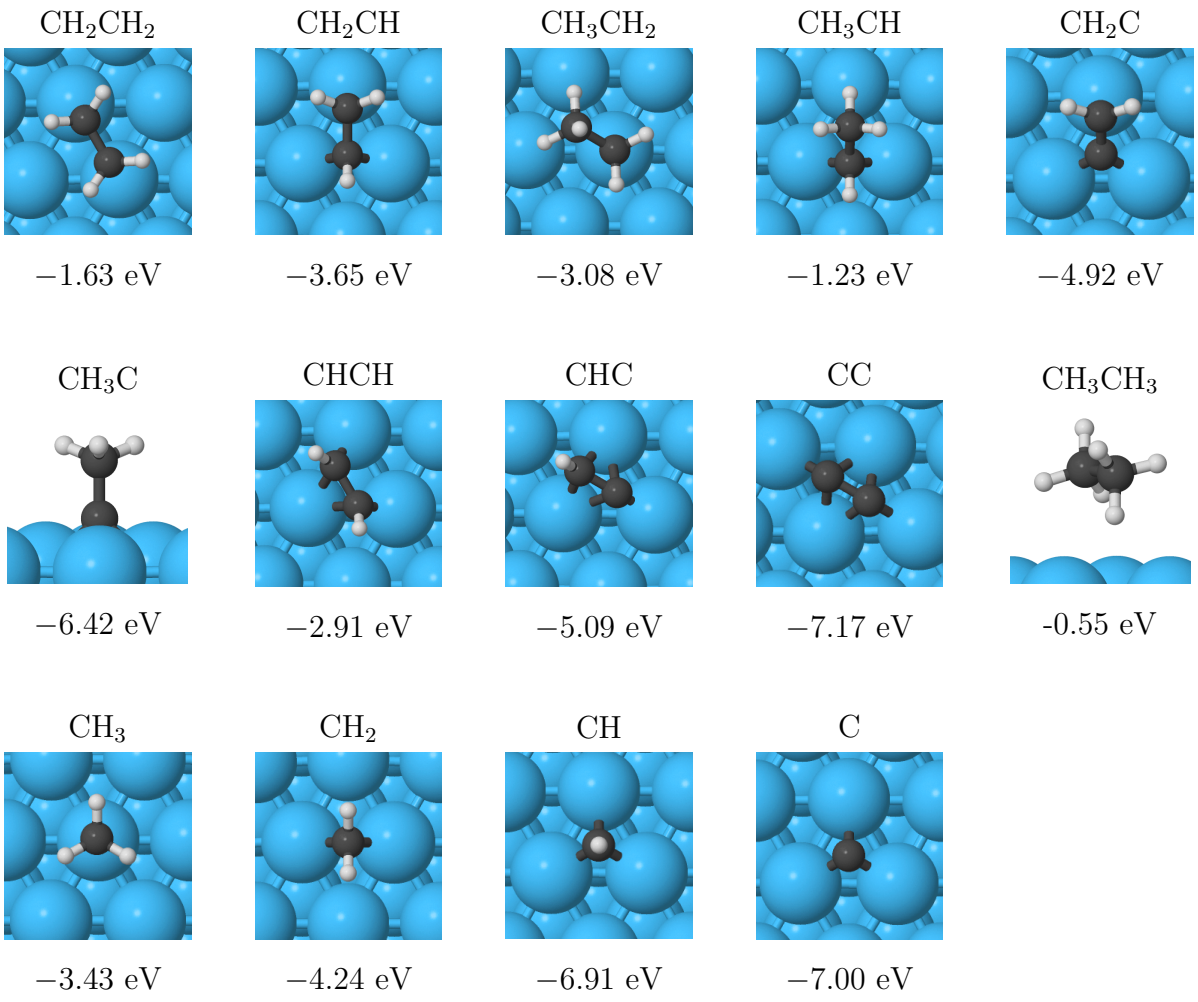

Figure 3: The lowest energy geometries of the hydrocarbon species adsorbed onto the Ir(111) surface. The adsorption energies of each species is also included. Ir atoms are shown in blue, while C and H are dark and light grey, respectively.

considering hydrogenation and dehydrogenation reactions one has to place a H atom next to the corresponding species for the initial and final states. The top site was found to be the most favourable binding site, with an adsorption energy that is 0.3 eV greater than that for the other sites.

Hence, when modelling hydrogenation and dehydrogenation reactions, we placed the H atoms at the most favourable top position some distance away from the molecule and optimised the geometry. Several such top positions relative to the hydrocarbon molecule were tried to find the lowest energy path; in some cases this affected the barriers by up to 0.5 eV. The calculated energy barriers for all reactions shown in Figure 2 (for both directions) are presented in Table 1. Note that in Figure 2 the direction of forward reactions is from left to right (or downward in the case of the C-C breaking reactions). The relaxed initial, transition and final state geometries for most of the reactions and the corresponding energy profiles are shown in the SI. In some cases, such as in reaction 1, more than one maxima appear corresponding to the H attachment/detachment and the diffusion away from or towards the parent species. In the case of the dehydrogenation reactions, once a H atom has been removed it is not retained for the next reaction step (except for the reverse hydrogenation reaction), and hence the final and initial states may be different for two subsequent reactions in the scheme of Figure 2.

The energy barriers for all the reactions lie in the range 0.3–2.5 eV. The isomerisation reactions 9, 10, and 15 have much higher barriers than the dehydrogenation and hydrogenation reactions, and will therefore be much less likely to occur. Generally, dehydrogenation reactions have lower barriers than hydrogenation reactions in most cases, apart from reactions 7, 11, 12, and 13. This trend might suggest that dehydrogenation reactions are favoured, eventually leading to the formation of pure carbon species C_n.

Our results also show that the barriers for C-C breaking are mostly of the order of 1–2 eV and are therefore quite high. However, for some of the species involved the barriers may be lower compared to the other possible processes and therefore they must be included in the reaction scheme. Breaking the C-C bond will inevitably lead to CH_m species and C monomers. Some of these may also become dehydrogenated or hydrogenated and therefore the barriers for these processes were also calculated. In addition, two monomeric carbon species can join together to reform the C-C bond, which can be described by the reverse of C-C breaking.

4.4 Interpretation of C 1s core level spectra

Each peak in XPS spectra corresponds to a particular C atom belonging to some C_nH_m species; hence, whether there are one or two spectral components due to a particular species depends on whether the C atoms have the same or different local atomic environment on the surface. Additional complications in this analysis arise from the fact that peaks may be accompanied by their vibrational satellites.

In order to give a detailed interpretation of the many components observable in the C 1s spectra during the annealing ramps, and hence to be able to deduce the ethylene conversion mechanism, we performed DFT calculations of the C 1s core level BEs for all the C_nH_m species, including final state effects due to the core-hole screening. The results in Figure 4, which shows

	Reaction in forward direction	E_f [eV]	E_b [eV]
1	$CH_2CH_2 \rightarrow CH_2CH + H$	0.39	0.58
2	$CH_2CH_2 + H \rightarrow CH_3CH_2$	0.70	0.35
3	$CH_2CH \rightarrow CH_2C + H$	0.35	0.66
4	$CH_2CH + H \rightarrow CH_3CH$	0.64	0.27
5	$CH_3CH_2 \rightarrow CH_3CH + H$	0.33	0.49
6	$CH_3CH_2 + H \rightarrow CH_3CH_3$	2.16	–
7	$CH_2C + H \rightarrow CH_3C$	0.82	0.99
8	$CH_3CH \rightarrow CH_3C + H$	0.46	1.48
9	$CH_2CH_2 \rightarrow CH_3CH$	1.39	1.20
10	$CH_2CH \rightarrow CH_3C$	1.37	2.01
11	$CHC + H \rightarrow CH_2C$	0.54	1.17
12	$CHC \rightarrow C\text{-}C + H$	1.23	0.65
13	$CHCH \rightarrow CHC + H$	1.23	0.58
14	$CHCH + H \rightarrow CH_2CH$	0.77	0.53
15	$CHCH \rightarrow CH_2C$	2.44	2.52
16	$CH_3 \rightarrow CH_2 + H$	0.50	0.58
17	$CH_2 \rightarrow CH + H$	0.09	0.83
18	$CH \rightarrow C + H$	1.11	0.66
CB1	$CH_2CH_2 \rightarrow CH_2 + CH_2$	1.45	0.61
CB2	$CH_3CH_2 \rightarrow CH_3 + CH_2$	1.56	1.47
CB3	$CH_3CH \rightarrow CH_3 + CH$	0.89	1.31
CB4	$CH_2CH \rightarrow CH_2 + CH$	1.07	1.44
CB5	$CH_2C \rightarrow CH_2 + C$	1.88	0.80
CB6	$CHCH \rightarrow CH + CH$	0.85*	1.15
CB7	$CHC \rightarrow CH + C$	0.73	1.29
CB8	$CC \rightarrow C + C$	1.18	1.29
H	$H + H \rightarrow H_2$	1.25	–

Table 1: The energy barriers for the various reactions numbered as in Figure 2. E_f is the energy barrier associated with the forward direction of the arrow, whereas E_b is the backward reaction barrier. Barriers for two adsorption reactions are not shown because these are deemed to be irrelevant to this study. * This is an estimated energy barrier, see SI for details.

that the relative core level shifts, reported with respect to molecular ethylene adsorbed on Ir, can be as large as 1.2 eV. Correspondingly, high-resolution and high-statistics C 1s core level spectra have been acquired after annealing to selected temperatures (see Figure 5(a)). The temperatures have been chosen from the TP-XPS data to be representative of the temperature ranges shown in Figure 1(d).

Note that, due to the approximate nature of the method proposed in Ref. [36] for calculating the core levels, only relative BEs are of significance; hence an alignment of the DFT calculated core level shifts with the experimental BE scale was performed. This has been achieved by requiring an energy match between the calculated BE for the C 1s core levels for CH_2C and experimental values obtained by fitting the low temperature high-resolution spectrum with Doniach-Šunjić (D-S) line shape [43] convoluted with a Gaussian. This particular species has been selected because, as follows from the DFT calculated energy barriers in Table 1 and the reaction scheme in Figure 2, at low temperatures the system will most likely progress by following reactions 1 and 3 to form CH_2C, and hence it is quite clear that this is the first and only stable species present on the surface after ethylene starts to dissociate. This species has two non-equivalent C atoms and hence accounts for two CLS core level components, as seen in the lowest curve in Figure 5(a). The low BE feature is assigned to molecular ethylene, which is also present, since the corresponding DFT calculated BE value falls close to its position. Observed deviations can be accounted for by considering the presence of a dense layer, with non-negligible lateral interactions, which can cause the C atoms within the molecules to be in slightly different local chemical environments. Once the alignment has been performed, the observed peaks can be assigned to specific species on the basis of the DFT calculated BE shifts, as reported in Figure 5(a).

For one chemical species a vibrational splitting of the core level is observed (Figure 5(b)) in the energy range compatible with the vibration of the C-H stretching mode. This split is characteristic of each chemical bond, and can be used as a fingerprint to determine the origin of a particular feature in the spectra. A fit of the CHCH spectrum, shown in Figure 5(b), has been performed with all the D-S line shape parameters constrained so that the vibrational replicas have the same line shape as the adiabatic peak itself. The splitting between the replicas has also been constrained so that all the replicas appear at equal energy intervals. This procedure leads to a low residual fit with a value for the vibrational energy loss of 405 meV, which is in good agreement with the DFT calculated C^*-H vibrational energy of 380 meV for CHCH with core-hole excited C atom (denoted C^*); C-H vibrational energies for other hydrocarbon species were found to be much lower (see the SI). This unequivocally identifies the chemical species in the orange spectrum of Figure 5(a) as CHCH, and also confirms the initial assignment, as the calculated BE for CHCH is the closest to that of the main (adiabatic) peak from the fit of the spectrum in Figure 5(b).

This allows us also to determine that for the spectrum at 450 K CH is present together with CHCH (the calculated BE of CH being the closest to the observed peak), and that at higher temperatures carbon clusters appear, as confirmed by the calculated BEs for carbon monomers and dimers, which coincide with observed peaks for the spectra acquired at 550 K.

In Figure 6(a) the integral intensities due to each chemical species, and therefore the relative

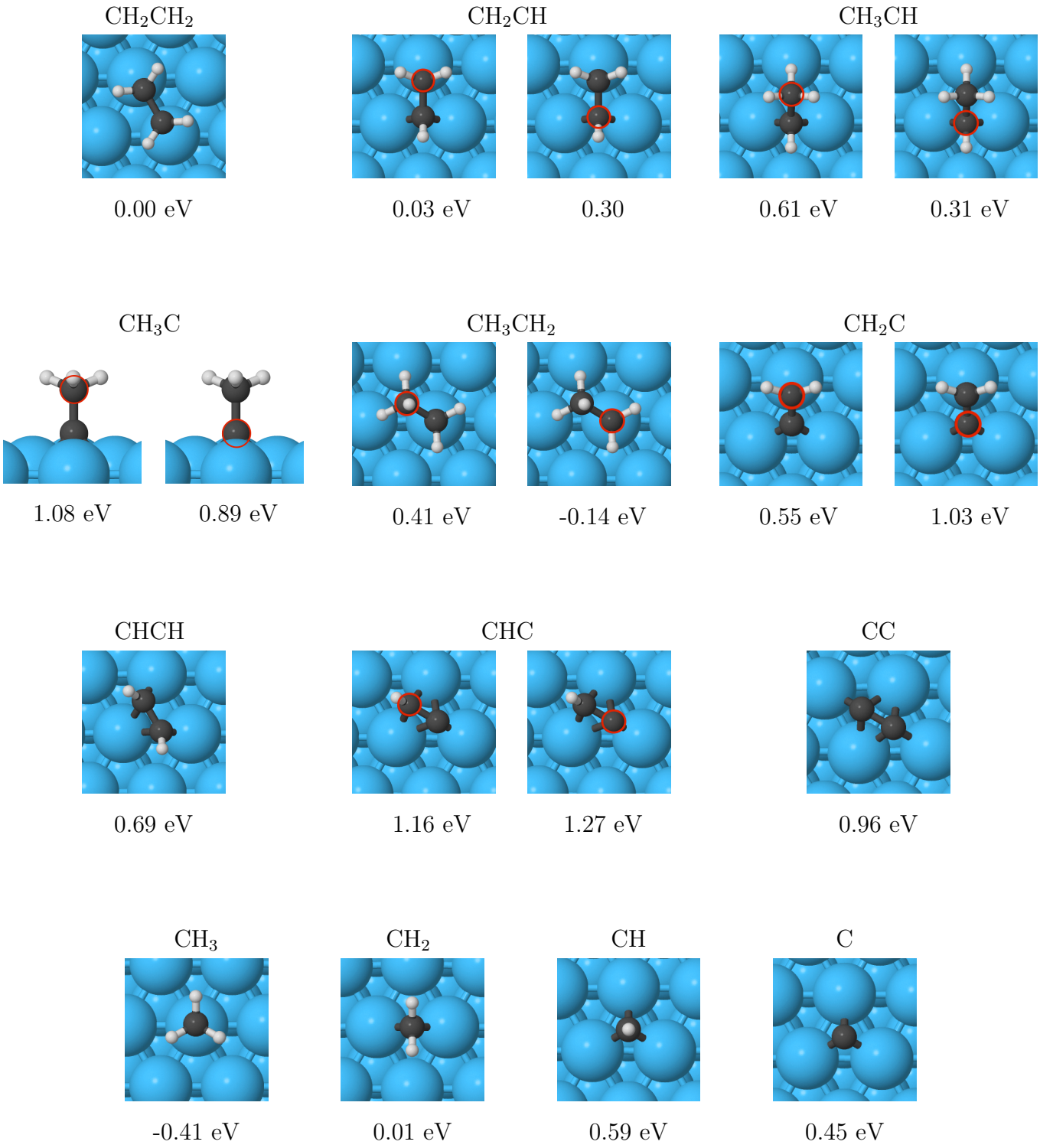

Figure 4: The 1s core level shift calculated for carbon atoms within all the different hydrocarbon species with respect to ethylene in the final state approximation. For two non-equivalent carbon atoms in the same molecule, two energies are given corresponding to the circled atoms in the left and right panels, respectively. For species where the C atoms appear in the same environment, E_{CLS} is the same only a single value is given.

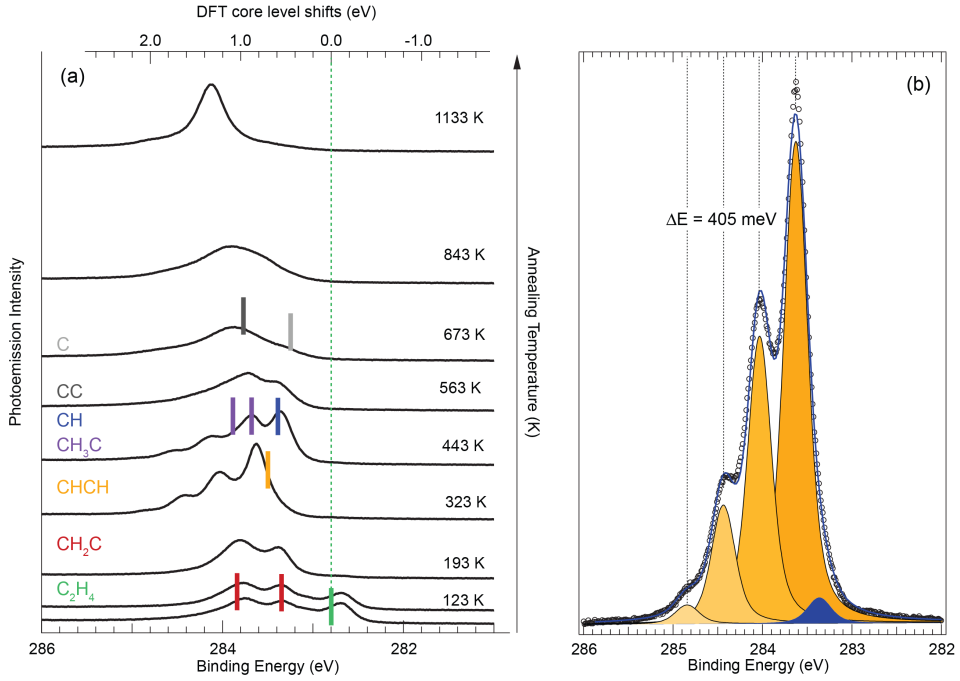

Figure 5: High-resolution and high-statistics XPS spectra acquired after annealing the ethylene covered substrate to selected temperatures. In (a), from the bottom upwards, spectra acquired after exposure at 90 K, and after annealing at increasing temperatures. The DFT calculated BEs for the species (shown on the left with different colours) found to be present on the surface have been marked with the same colour ticks. In (b), a fit of the spectrum acquired after annealing the system to 323 K is shown. This spectrum shows, besides the main adiabatic peak, a series of vibrational replicas, whose splitting was found to be 405 meV. A small amount of CH (blue peak) is also detected already at this temperature.

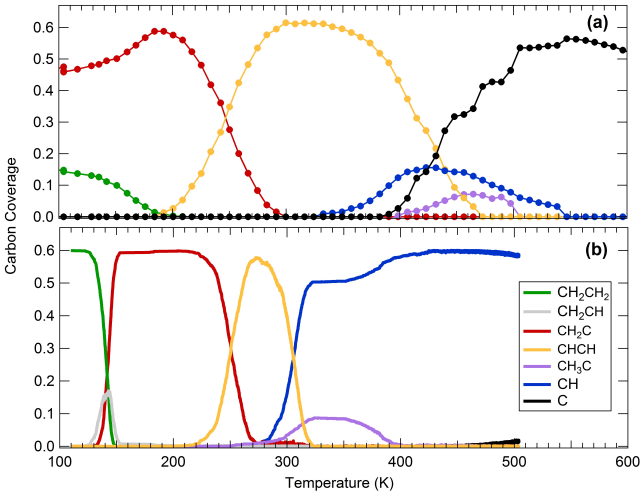

Figure 6: The deduced concentration of the principal species on the surface as a function of temperature (which is ramped up linearly with time at a rate of 1.5 Ks^{-1}) starting from a ethylene coverage of 0.6 ML. (a) experimental results. (b) kMC simulated coverages

abundances on the surface, are plotted as a function of the temperature.

In the first part of the analysis, the high resolution data (Figure 5) have been fitted by D-S functions in order to extract the spectral line shape characteristic of each chemical species. Each chemical species is represented by one or two peaks associated with the number of non-equivalent C atoms, and the peak positions are characterised by the DFT-obtained BEs. The only exception is CHCH, for which vibrational replicas also exist (all the replicas have the same line shape and identical BE splitting), as well as various C_n species present at high temperatures. In the latter case the integral intensity was evaluated cumulatively for all the carbon-only species.

In the second step, the time-resolved data have been individually fitted with a sum of the normalised spectra obtained as described above. In order to obtain the best fit to the data, each spectrum was multiplied by a factor that is, in fact, proportional to the relative amount of the species on the surface, while keeping the species' spectrum shape fixed. The binding energy of each species' spectrum as a whole was allowed to vary, with respect to the value found for the high resolution spectra, within a small energy range (<0.1 eV) in order to account for lateral interactions between different species. In the case of atoms (Oxygen-[44]) and light molecules (carbon monoxide-[45]) it was found that core electron binding energies display a slight change as a function of adsorbate coverage due to mutual interaction that can be of the order of 100 meV (110 meV for O on Rh(111) [44], 180 meV for CO on Pd(111) [45]), even when the adsorption site is unchanged (see also the SI). The integrated final spectral peaks at each temperature represent relative concentrations of the species. Some variations in the total integral intensity of the C 1s peak were observed, especially in the temperature intervals where CHCH and CH are present, leading to a slight increase in the overall C signal, contrary to the expected constant value corresponding to the initial number of C atoms on the surface. We interpret this increase in intensity to be due to photoelectron diffraction effects when local ordering of the species is improved. To counteract this increase, which cannot be due to an

increase of the C surface density, a normalisation constant of 0.66 was used for the signal of CH and CHCH. Concentrations obtained in this way are plotted as a function of annealing temperature in Figure 6(a).

The data suggests the following reaction mechanism. First, CH_2C is formed already at 90 K (molecular ethylene being observed only at higher coverages), which converts completely into CHCH; in turn, CHCH dissociates to CH monomers, which dehydrogenate to produce atomic C and hydrogen. Above 400 K, a small amount of CH_3C is formed from rehydrogenation of CHCH, which reacts with atomic H species found on the surface. It is worth mentioning that the formation of CH_3C from ethylene on Ir(111) has been suggested by Marinova et al. [46]

The derived reaction path during the temperature ramp, based mostly on core level photoemission spectra and DFT calculated BEs, can be compared to the one deduced following the direction of the reactions with the lowest DFT energy barriers (Table 1). Specifically, since our experiments begin from a relatively low temperature, initially the system will likely progress by following reactions 1 and 3 to form CH_2C corresponding to low dehydrogenation reaction barriers. This fully agrees with the CH_2C concentration evolution shown in Figure 6.

With an increase of temperature, five possible pathways become available for CH_2C: it can hydrogenate to either CH_2CH or CH_3C, dehydrogenate to CHC, isomerise to CHCH or undergo C-C breaking to form CH_2 and C. The hydrogenation reactions 3-reversed and 7 have the lowest barriers of these (0.66 eV and 0.82 eV respectively), and will therefore act as the main competing pathways out of CH_2C. If reaction 7 were followed, CH_3C, which is not observed experimentally at temperatures where CH_2C is present, would have been produced and remained stable for some considerable range of temperatures as the lowest barrier out of this species is the reverse reaction back to CH_2C, which is still high (0.99 eV). If reaction 3 is followed, then CH_2CH is formed. As the barrier back to CH_2C is very small it is likely that this species will immediately dehydrogenate backwards to CH_2C, resulting in a short lifetime to these species and explaining why CH_2CH is not observed experimentally. There is in any case a possibility that some portion of the CH_2C species should follow reaction 14 instead, leading to CHCH. The species evolution curves presented in Figure 6 (a) and (b) show that the latter route ($CH_2C \rightarrow CH_2CH \rightarrow CHCH$) appears to be preferable of the two.

We next see in Figure 6 (a) that as the concentration of CHCH starts decreasing, CH appears. This is explained by the fact that the reaction with the lowest barrier starting from CHCH is the C-C breaking reaction, CB6, leading to CH species. At even higher temperatures formation of carbon clusters C_n is detected as shown in Figure 6(a) . In order to corroborate these results we have performed a kinetics analysis since there are many competing processes leading to either dehydrogenation of CH to give carbon monomers (reaction 17) or CH disappearance due to reactions 18, CB3, CB4, CB6 and CB7 followed by the formation of other species. Therefore, a calculation that takes account of all competing processes is required, especially since at high temperatures many of the barriers can be easily overcome.

4.5 Kinetic Monte Carlo simulations of species evolution

The interpretation suggested above was based entirely on the core level shifts and derived experimental evolution of species at each temperature, evaluated from the calculated energy barriers and possible reaction pathways. To validate this interpretation and the proposed reaction mechanism, the kinetics of all processes depicted in Figure 2 need to be considered, which takes account of the relative abundance of all species at each time during the temperature ramp, their spatial distribution and of all the competing processes. This needs to be supplemented by the fact that during the growth process hydrogen atoms adsorbed on the surface may also be lost by the formation of hydrogen molecules. This can occur when the H atoms are mobile enough to come close together on the surface, i.e. at higher temperatures. The desorption of H_2 will reduce the availability of hydrogen atoms on the surface, acting as a limiting factor for the hydrogenation reactions. The energy barrier for the formation of an H_2 molecule from two adsorbed H atoms was calculated to be 1.25 eV. The highest barrier calculated for H diffusion was 0.36 eV, which is small in view of the temperatures used in our experiments. Therefore at higher temperatures H is likely to diffuse easily on the surface, form H_2 and desorb. Understanding H diffusion is also important for assessing the likelihood that the H atoms, when detached from the hydrocarbon species, are able to move away from them instead of recombining, as the latter will inhibit the overall dehydrogenation processes. The diffusion of H are provided in the SI.

To reveal the kinetics of the complicated ethylene conversion reactions and obtain the time evolution of the concentrations of various species on the surface that can be compared with experimental results of Figure 6(a) deduced from the XPS spectra, we performed kinetic Monte Carlo (kMC) simulations. A grid-based model was devised to incorporate the geometries of all the relaxed hydrocarbons shown in Figure 3. These are allowed to undergo the reactions as listed in Figure 2 as well as diffuse on the surface.

In calculating the rates for the reactions in the kMC simulations we have to determine, apart from the energy barriers, the attempt frequencies as well. We used a typical value of $\nu = 10^{13}$ s^{-1} for most reactions apart from 3, 7, 14 and CB6, where correctly determining the attempt frequencies is important, since they play a major role in the reaction pathway, as indicated by the experimental BEs and the DFT energy barriers. In the latter cases we calculated the pre-exponential factors explicitly using Vineyard's formula [21], as reported in the SI; these frequencies are in the range of 10^{12}-10^{13} s^{-1}.

The kMC simulations are performed to give the surface coverages of the various species as a function of time, starting from an initial ethylene concentration corresponding to 0.6 ML of C atoms (and zero coverage for other species), as the temperature is increased linearly at a rate of 1.5 Ks^{-1}. The calculated evolution of species concentrations depicted in Figure 6(b) demonstrates reasonable agreement with the high coverage experimental results in Figure 6(a). We observe the same order of species appearing as the temperature is increased. The main noticeable deviations from the experimental results concern the narrower temperature window for the intermediate species CHCH and the much larger window for CH. We also find that CH_3C is present between 300 and 400 K in the theory, however in the experiment it appears between 400 and 500 K. Finally, there is also an absence of partially dissociated ethylene at 90 K in the

calculated evolution. This is probably due to the fact that the barrier for CH_2CH_2 to CH_2CH dehydrogenation reaction is somewhat overestimated in our calculations.

These differences can be in part explained by the lateral interactions between species that can not be accounted for with the kMC simulations. At high coverages neighbouring species will interact strongly with each other, which will affect the energy barriers of the reactions (as discussed in the SI). This will give rise to different lifetimes for certain species. It should also be mentioned that small errors in the DFT energy barriers can affect the kMC deduced species coverages. We find in our simulations that due to the nature of the reaction rates even very small changes in the calculated energy barriers can somewhat affect the results of the simulations. This becomes particularly problematic when two competing processes have similar barriers. For example, the hydrogenation of CHCH to CH_2CH has a barrier of 0.77 eV, which is near to the energy barrier for CHCH to break into CH (0.85 eV). Small errors in these energy barriers can greatly affect the lifetime of CHCH and whether it can hydrogenate to CH_2CH, which allows CH_3C to be produced. For this reason at present it may be quite challenging to perform precise simulations of the time evolution of species coverages and compare them with those determined from the XPS experiments. The impact of changes to the energy barriers on the species coverages is discussed in detail in the SI, whereby altering the barriers slightly to take account of these effects is shown to result in a stronger agreement with the experimentally deduced coverages.

Detailed data on species concentrations in conjunction with the reaction scheme of Figure 2 enable us to characterise the reaction pathway as follows. Soon after starting at 130 K there is a drop in the concentration of ethylene (CH_2CH_2) which is matched by an increase in vinylidene (CH_2C). This suggests that two dehydrogenation reactions 1 ($CH_2CH_2 \rightarrow CH_2CH+H$) and 3 ($CH_2CH \rightarrow CH_2C+H$) take place quickly once ethylene has been deposited, and that the second occurs immediately after the first, so that vinyl (CH_2CH) is not stable for long enough to show a significant concentration signature. However, the CH_2C concentration begins to decrease at about 210 K due to the hydrogenation reaction (reverse reaction 3) leading back to CH_2CH followed immediately by the dehydrogenation reaction to acetylene (CHCH) (reaction 14). For CHCH the barrier for C-C breaking is sufficiently low ($\approx$ 0.85 eV) such that methylidyne (CH) can be generated at around 270 K. A small amount of the CHCH may be converted to CH_3C via its hydrogenation to CH_2CH and then the removal and addition of the H atom to form CH_3C. This happens at around 300 K. Eventually by 400 K this converts to CH by the reverse process. Afterwards CH becomes the only species present until C monomers start forming at 500 K. The decrease in CH is matched with the increase in C monomers. Hence, as the temperature increases CH can be dehydrogenated to C. However since the reverse reaction is more favourable C only starts forming once H atoms are lost due to the formation of H_2 molecules. The long survival for CH compared to the experimental results could be due to overestimation of the H_2 desorption barrier by DFT calculations, which assumes the low coverage limit.

5 Conclusions

In this paper a comprehensive approach based on XPS experiments, DFT calculations and a kinetic Monte Carlo simulation has been applied to acquire a detailed understanding of the mechanism of ethylene decomposition on the Ir(111) surface in TPG experiments widely used for growing graphene on transition metal surfaces. The combined approach presented here suggests the following pathway for ethylene decomposition with eventual formation of carbon monomer species:

$CH_2CH_2 \rightarrow CH_2CH + H$

$CH_2CH \longleftrightarrow CH_2C + H$

$CH_2CH \rightarrow CHCH + H$

$CHCH \rightarrow CH + CH$

$CH \rightarrow C + H.$

In the proposed reaction pathway we find that hydrogenation, dehydrogenation and C-C breaking reactions are required in order to produce carbon. An important feature of this pathway is that the C-C bond is broken in order to form carbon monomers and this happens before the molecule is fully dehydrogenated. Breaking of the C-C bond allows for the possibility that graphene is formed from carbon clusters that are predominantly built from C monomers and not dimers. The clusters may then contain an odd number of C atoms, and this is in agreement with experimental work which has observed that the rate of graphene growth from ethylene feedstock is proportional to the carbon monomer concentration to the power of five [3, 47, 1]. This suggests that the graphene grows through the addition of five atom carbon clusters, which would not be possible without C-C bond breaking. [48]

We believe that this is the first study ever made in which such a detailed investigation of the reactions sequence of ethylene decomposition has been attempted based on a comprehensive interplay of several experimental and theoretical techniques complementing each other. In the theoretical study of the decomposition of C_nH_m species on the Pt(111) and Pt(210) surfaces conclusions about the decomposition mechanism were made based only on the energy barriers for the reactions. [19, 20] This approach lacked any calculation of the kinetics of the decomposition, which depends on the temperature and the concentration of the various species. Here we have shown that this is necessary in order to determine the correct evolution. Similarly in kinetic Monte Carlo calculations performed for the reactions of ethylene on the Pt(111) surface [16] only a subset of all possible reactions were considered, and without experimental insight it was suggested that CH_3C is formed from the hydrogenation of CH_2C during the decomposition. However our combined XPS and theory results find that, on Ir(111), CHCH is the intermediate species formed after CH_2C, which can only be understood within the approach based on the complete reaction scheme combined with kinetics based simulations.

From monomer carbon atoms, freely diffusing on the surface, carbon dimers and bigger C_n clusters can be formed, which eventually leads to nucleation and growth of graphene. Although this later stage of graphene formation lies beyond the scope of this study, which is devoted exclusively to the first stages of graphene growth related to hydrocarbon decomposition at intermediate temperatures, a direct extension of this study would be to include reactions related

to formation, decomposition and transformation of larger carbon clusters and C_nH_m species which are essential for later stages of graphene growth taking place at higher temperatures. We believe that such an extension of the present study, which should also rely on closely linked experiment and theory, may even address the question of what is the optimum annealing protocol for ethylene decomposition with the aim of forming large graphene sheets with a minimum number of defects. The proposed reaction scheme and reaction parameters can now be applied to other experimental scenarios widely used for graphene growth via ethylene decomposition, e.g. for considering the decomposition process during ethylene evaporation on a hot Ir surface.

It is clear that for other types of hydrocarbon feedstock the reaction scheme and hence the corresponding reaction path could be very different. The species produced in the later stages of the molecular decomposition might be more complex than the carbon monomers found for ethylene on Ir(111) in the present study. In particular, various carbon clusters might be generated, such as dimers or six-member rings (e.g. when using benzene), or even larger carbon molecules (when using coronene [49]). This will affect the graphene growth kinetics and (possibly) its defectiveness. The choice of hydrocarbon feedstock has been shown to influence the initial stages of growth: for example, when using benzene, graphene is produced at a lower temperature compared with studies using methane. [50] The joint experimental and theoretical approach developed here should prove to be extremely useful in uncovering the preferential reaction path in each case and understanding the nature of the fragments, left after the decomposition of the molecules, that subsequently act as the growth precursors, particularly with regard to the number of carbon atoms in the fragments.

6 Acknowledgement

Through our membership of the UK's HPC Materials Chemistry Consortium, which is funded by EPSRC (grants EP/F067496, EP/L000202), this work made use of the facilities of HECTOR and ARCHER, the UK's national high-performance computing service, which is funded by the Office of Science and Technology through EPSRC's High End Computing Programme. J. P. was supported through a studentship in the Centre for Doctoral Training on the Theory and Simulation of Materials at Imperial College London funded by EPSRC under grant number EP/G036888/. We acknowledge the financial support from MIUR through the project PRIN entitled "GRAF. Frontiers in graphene research: understanding and controlling advanced functionalities" (N.20105ZZYSE001) and from the University of Trieste through the programme "Finanziamento di Ateneo per progetti di ricerca scientifica - FRA 2014".

References

[1] H. Tetlow, J. Posthuma de Boer, I. J. Ford, D. Vvedensky, J. Coraux, and L. Kantorovich. Growth of epitaxial graphene: Theory and experiment. *Physics Reports*, 542:195–295, 2014.

[2] J. Coraux, A. T. N'Diaye, M. Engler, C. Busse, D. Wall, N. Buckanie, F-J. Meyer zu Heringdorf, R. van Gastel, B. Poelsema, and T. Michely. Growth of graphene on Ir(111). *New Journal of Physics*, 11:023006, 2009.

[3] E. Loginova, N. C. Bartelt, P. J. Feibelman, and K. F. McCarty. Evidence for growth by C cluster attachment. *New Journal of Physics*, 10:093026, 2008.

[4] C. Hwang, K. Yoo, S. J. Kim, E. K. Seo, H. Yu, and L. P. Biro. Initial stage of graphene growth on a Cu substrate. *Journal of Physical Chemistry C*, 115(45):22369–22374, 2011.

[5] B. Wang, X. Ma, M. Caffio, R. Schaub, and W.-X. Li. Size-selective carbon nanoclusters as precursors to the growth of epitaxial graphene. *Nano Letters*, 11:424–430, 2011.

[6] J. Gao, J. Yip, J. Zhao, Boris I. Yakobson, and F. Ding. Graphene nucleation on transition metal surface: Structure transformation and role of the metal step edge. *Journal of the American Chemical Society*, 133(13):5009–5015, 2011.

[7] L. Huang, W-Y. Xu, Y-D. Que, Y. Pan, M. Gao, L-D. Pan, H-M. Guo, Y-L. Wang, S-X. Du, and H-J. Gao. The influence of annealing temperature on the morphology of graphene islands. *Chinese Physics B*, 21(8):088102, 2012.

[8] Y. Cui, Q. Fu, H. Zhang, and X. Bao. Formation of identical-size graphene nanoclusters on Ru(0001). *Chem. Commun.*, 47:1470–1472, 2011.

[9] G. C. Dong, D. W. van Baarle, M. J. Rost, and J. W. M. Frenken. Graphene formation on metal surfaces investigated by in-situ scanning tunneling microscopy. *New Journal of Physics*, 14:053033, 2012.

[10] E. Miniussi, M. Pozzo, A. Baraldi, E. Vesselli, R. R. Zhan, G. Comelli, T. O. Menteş, M. A. Niño, A. Locatelli, S. Lizzit, et al. Thermal stability of corrugated epitaxial graphene grown on Re (0001). *Physical Review Letters*, 106(21):216101, 2011.

[11] S. Lizzit and A. Baraldi. High-resolution fast X-ray photoelectron spectroscopy study of ethylene interaction with Ir(111): From chemisorption to dissociation and graphene formation. *Catalysis Today*, 154:68 – 74, 2010.

[12] A. Baraldi, G. Comelli, S. Lizzit, M. Kiskinova, and G. Paolucci. Real-time x-ray photoelectron spectroscopy of surface reactions. *Surface Science Reports*, 49(6):169–224, 2003.

[13] P. Lacovig, M. Pozzo, D. Alfe, P. Vilmercati, A. Baraldi, and S. Lizzit. Growth of dome-shaped carbon nanoislands on ir (111): the intermediate between carbidic clusters and quasi-free-standing graphene. *Phys. Rev. Lett.*, 103(16):166101, 2009.

[14] W. Zhang, P. Wu, Z. Li, and J. Yang. First-principles thermodynamics of graphene growth on Cu surfaces. *Journal of Physical Chemistry C*, 115(36):17782–17787, 2011.

[15] G. Gajewski and C. W. Pao. Ab initio calculations of the reaction pathways for methane decomposition over the Cu (111) surface. *Journal of Chemical Physics*, 135(6):064707, 2011.

[16] H. A. Aleksandrov, L. V. Moskaleva, Z-J. Zhao, D. Basaran, Z-X. Chen, D. Mei, and N. Rösch. Ethylene conversion to ethylidyne on Pd(111) and Pt(111): A first-principles-based kinetic Monte Carlo study. *Journal of Catalysis*, 285(1):187 – 195, 2012.

[17] Z-J Zhao, L. V. Moskaleva, H. A. Aleksandrov, D. Basaran, and N. Rösch. Ethylidyne formation from ethylene over pt(111): A mechanistic study from first-principle calculations. *Journal of Physical Chemistry C*, 114(28):12190–12201, 2010.

[18] D. Basaran, H. A. Aleksandrov, Z-X. Chen, Z-J. Zhao, and N. Rösch. Decomposition of ethylene on transition metal surfaces m(111). a comparative DFT study of model reactions for m=pd, pt, rh, ni. *Journal of Molecular Catalysis A: Chemical*, 344:37, 2011.

[19] Ying Chen and Dionisios G. Vlachos. Hydrogenation of ethylene and dehydrogenation and hydrogenolysis of ethane on pt(111) and pt(211): A density functional theory study. *Journal of Physical Chemistry C*, 114(11):4973–4982, 2010.

[20] R. M. Watwe, R. D. Cortright, J. K. Nørskov, and J. A. Dumesic. Theoretical studies of stability and reactivity of c2 hydrocarbon species on pt clusters, pt(111), and pt(211). *Journal of Physical Chemistry B*, 104(10):2299–2310, 2000.

[21] G. H. Vineyard. Frequency factors and isotope effects in solid state rate processes. *Journal of Physics and Chemical of Solids*, 3:121, 1957.

[22] P. Hänggi, P. Talkner, and M. Borkovec. Reaction-rate theory: fifty years after kramers. *Reviews of Modern Physics*, 62:251 – 341, 1990.

[23] M. Bianchi, D. Cassese, A. Cavallin, R. Comin, F. Orlando, L. Postregna, E. Golfetto, S. Lizzit, and A. Baraldi. *New Journal of Physics*, 11:063002, 2009.

[24] H. Jónsson, G. Mills, and K. W. Jacobsen. *Classical and Quantum Dynamics in Condensed Phase Simulations*, chapter Nudged Elastic Band Method for Finding Minimum Energy Paths of Transitions. World Scientific, 1998.

[25] G. Mills, H. Jónsson, and G. K. Schenter. Reversible work transition state theory: Application to dissociative adsorption of hydrogen. *Surface Science*, 324(2-3):305–337, 1995.

[26] G. Henkelman and H. Jónsson. Improved tangent estimate in the nudged elastic band method for finding minimum energy paths and saddle points. *Journal of Chemical Physics*, 113:9978, 2000.

[27] G. Henkelman, B. P. Uberuaga, and H. Jónsson. A climbing image nudged elastic band method for finding saddle points and minimum energy paths. *Journal of Chemical Physics*, 113(22):9901–9904, 2000.

[28] J. Hutter, M. Iannuzzi, F. Schiffmann, and J. VandeVondele. cp2k: atomistic simulations of condensed matter systems. *Wiley Interdisciplinary Reviews: Computational Molecular Science*, 4(1):15–25, 2014.

[29] S. Goedecker, M. Teter, and J. Hutter. Separable dual-space gaussian pseudopotentials. *Physical Review B*, 54:1703–1710, Jul 1996.

[30] J. P. Perdew, K. Burke, and M. Ernzerhof. Generalized gradient approximation made simple. *Phys. Rev. Lett.*, 77:3865–3868, Oct 1996.

[31] S Grimme, J Antony, S Ehrlich, and H Krieg. A consistent and accurate ab initio parametrization of density functional dispersion correction (dft-d) for the 94 elements h-pu. *Journal of Chemical Physics*, 132(15):154104, 2010.

[32] J. VandeVondele and J. Hutter. Gaussian basis sets for accurate calculations on molecular systems in gas and condensed phases. *Journal of Chemical Physics*, 127(11):114105, 2007.

[33] S.F. Boys and F. Bernardi. The calculation of small molecular interactions by the differences of separate total energies. some procedures with reduced errors. *Mol. Phys.*, 19:553, 1970.

[34] A.B. Bortz, M.H. Kalos, and J.L. Lebowitz. A new algorithm for monte carlo simulation of ising spin systems. *Journal of Computational Physics*, 17(1):10 – 18, 1975.

[35] A. Prados, J. J. Brey, and B. Sánchez-Rey. A dynamical monte carlo algorithm for master equations with time-dependent transition rates. *Journal of Statistical Physics*, 89(3):709–734.

[36] Lukas Köhler and Georg Kresse. Density functional study of co on rh(111). *Phys. Rev. B*, 70:165405, Oct 2004.

[37] A. Baraldi, G. Comelli, S. Lizzit, D. Cocco, G. Paolucci, and R. Rosei. Temperature programmed x-ray photoelectron spectroscopy: a new technique for the study of surface kinetics. *Surface Science*, 367(3):L67–L72, 1996.

[38] M.B. Hugenschmidt, P. Dolle, J. Jupille, and A. Cassuto. Ethylene π species on bare and cesiated pt (111) surfaces. *Journal of Vacuum Science & Technology A*, 7(6):3312–3316, 1989.

[39] J.N. Andersen, A. Beutler, S.L. Sorensen, R. Nyholm, B. Setlik, and D. Heskett. Vibrational fine structure in the c 1s core level photoemission of chemisorbed molecules: ethylene and ethylidyne on rh(111). *Chemical Physics Letters*, 269:371, 1997.

[40] H.P. Steinrück, T. Fuhrmann, C. Papp, B. Tränkenschuh, and R. Denecke. *Journal of Chemical Physics*, 125:204706, 2006.

[41] B. E. Nieuwenhuys, D. I. Hagen, G. Rovida, and G. A. Somorjai. *Surface Science*, 59:155–176, 1976.

[42] F Zaera and N Bernstein. *Journal of the American Chemical Society*, 116:4881–4887, 1994.

[43] S. Doniach and M. Sunjic. Many-electron singularity in x-ray photoemission and x-ray line spectra from metals. *Journal of Physics C: Solid State Physics*, 3(2):285, 1970.

[44] M. V. Ganduglia-Pirovano, M. Scheffler, A. Baraldi, S. Lizzit, G. Comelli, G. Paolucci, and R. Rosei. Oxygen-induced rh $3d_{5/2}$ surface core-level shifts on rh(111). *Phys. Rev. B*, 63:205415, 2001.

[45] S. Surnev, M. Sock, M.G. Ramsey, F.P. Netzer, M. Wiklund, M. Borg, and J.N. Andersen. CO adsorption on Pd(1 1 1): a high-resolution core level photoemission and electron energy loss spectroscopy study . *Surface Science*, 470:171 – 185, 2000.

[46] Ts. S. Marinova and D. V. Chakarov. *Surface Science*, 192:275–282, 1987.

[47] E. Loginova, N. C. Bartelt, P. J. Feibelman, and K. F. McCarty. Factors influencing graphene growth on metal surfaces. *New Journal of Physics*, 11:063046, 2009.

[48] A. Zangwill and D. Vvedensky. Novel growth mechanism of epitaxial graphene on metals. *Nano Letters*, 11:2092–2095, 2011.

[49] D. Curcio, L. Omiciuolo, M. Pozzo, P. Lacovig, S. Lizzit, N. Jabeen, L. Petaccia, D. Alfè, and A. Baraldi. Molecular lifting, twisting, and curling during metal-assisted polycyclic hydrocarbon dehydrogenation. *Journal of the American Chemical Society*, 138(10):3395–3402, 2016. PMID: 26829531.

[50] Z. Li, P. Wu, C. Wang, X. Fan, W. Zhang, X. Zhai, C. Zeng, Z. Li, J. Yang, and J. Hou. Low-temperature growth of graphene by chemical vapor deposition using solid and liquid carbon sources. *ACS Nano*, 5(4):3385–3390, 2011.